A&A 433, 917–929 (2005)
DOI: 10.1051/0004-6361:20041113

Astronomy & Astrophysics

Spatial dependence of 2MASS luminosity and mass functions in the old open cluster NGC 188

C. Bonatto[1], E. Bica[1], and J. F. C. Santos Jr[2]

[1] Universidade Federal do Rio Grande do Sul, Instituto de Física, CP 15051, Porto Alegre 91501-970, RS, Brazil
e-mail: charles@if.ufrgs.br
[2] Universidade Federal de Minas Gerais, ICEx, Departamento de Física, CP 702, Belo Horizonte 30162-970, MG, Brazil

Received 16 April 2004 / Accepted 10 December 2004

Abstract. Luminosity and mass functions in the old open cluster NGC 188 are analysed by means of J and H 2MASS photometry, which provides uniformity and spatial coverage for a proper background subtraction. With an age of about 6–8 Gyr, NGC 188 is expected to be suffering the effects of advanced dynamical evolution. Indeed, previous works in optical bands have suggested the presence of mass segregation. Within the uncertainties, the observed projected radial density profile of NGC 188 departs from the two-parameter King model in two inner regions, which reflects the non-virialized dynamical state and possibly, some degree of non-sphericity in the spatial shape of this old open cluster. Fits with two and three-parameter King models to the radial distribution of stars resulted in a core radius $R_{\rm core} = 1.3 \pm 0.1$ pc and a tidal radius $R_{\rm tidal} = 21 \pm 4$ pc, about twice as large as the visual limiting radius. The concentration parameter $c = 1.2 \pm 0.1$ of NGC 188 makes this open cluster structurally comparable to the loose globular clusters. The present 2MASS analysis resulted in significant slope variations with distance in the mass function $\phi(m) \propto m^{-(1+\chi)}$, being flat in the central parts ($\chi = 0.6 \pm 0.7$) and steep in the cluster outskirts ($\chi = 7.2 \pm 0.6$). The overall mass function has a slope $\chi = 1.9 \pm 0.7$, slightly steeper than a standard Salpeter mass function. In this context, NGC 188 is similar to the 3.2 Gyr, dynamically evolved open cluster M 67. Solar metallicity Padova isochrone fits to the near-infrared colour-magnitude diagram of NGC 188 resulted in an age of 7.0 ± 1.0 Gyr. The best fit, obtained with the 7.1 Gyr isochrone, produced a distance modulus $(m - M)_0 = 11.1 \pm 0.1$, $E(B - V) = 0.0$, and a distance to the Sun $d_\odot = 1.66 \pm 0.08$ kpc. The observed stellar mass (in the range 0.98 $M_\odot$–1.08 $M_\odot$) in NGC 188 is $m_{\rm obs} = 380 \pm 12\ M_\odot$. A simple extrapolation of the observed overall mass function to stars with 0.08 $M_\odot$ resulted in a total present mass of $m_{\rm tot} \sim (1.8 \pm 0.7) \times 10^4\ M_\odot$. On the other hand, for a more realistic initial mass function which flattens in the low-mass range, the total mass in NGC 188 drops to $m_{\rm tot} \sim (3.8 \pm 1.6) \times 10^3\ M_\odot$. Since mass-loss processes such as evaporation and tidal stripping have been occurring in this old open cluster for about 7 Gyr, the primordial mass in NGC 188 must have been significantly larger than $\sim 4 \times 10^3\ M_\odot$. We also examined the consequences of the presence of unresolved binaries and concluded that, even if dominant in the CMD, binaries alone are not responsible for the flat central mass function, which supports the mass-segregation scenario.

Key words. Galaxy: open clusters and associations: individual: NGC 188

1. Introduction

With an age of about 7 Gyr (e.g. Carraro & Chiosi 1994), NGC 188 is one of the oldest known open clusters in the Galaxy. Located relatively far from the disk, its field is neither heavily contaminated by background stars nor obscured by dust, and contains a few hundreds of member stars. These conditions make NGC 188 an excellent laboratory for testing modern theories of stellar and dynamical evolution of star clusters.

The main effects related to the dynamical evolution of an open cluster are (i) mass segregation; (ii) tidal stripping and disruption by the Galactic gravitational field; and (iii) interactions with the disk, since a typical open cluster at the solar radius will cross the Galactic plane 10–20 times before being disrupted (de la Fuente Marcos 1998). Evaporation of a cluster may result from two-body relaxation processes, in which several stars can acquire positive energy during the closest approaches and eventually leave the cluster. Mass-loss during the course of stellar evolution and encounters with giant molecular clouds (e.g. Wielen 1991) also contribute to reducing a cluster's lifetime. Considering all these factors, the destruction time-scale for open clusters in the solar neighbourhood is about 600 Myr (Bergond et al. 2001). Consequently, only the most massive open clusters or those located at large Galactic radii are expected to survive longer than a few Gyr (Friel 1995). Indeed, de la Fuente Marcos (1998) has shown that the Milky Way should host several hundred thousands of open cluster remnants which have been disrupted both by the Galaxy and their own dynamical evolution.

Taking into account all of the above factors, as well as its location in the Galaxy, the dynamical evolution of NGC 188

should be essentially associated to mass segregation, evaporation and tidal stripping by the Galactic gravitational field.

As a consequence of mass segregation, the central regions of the more evolved clusters should present a main sequence (MS) depleted of low-mass stars, thus creating a core rich in compact and giant stars (Takahashi & Portegies Zwart 2000). Also, the luminosity (or mass) function (hereafter LF and MF) of a dynamically evolved open cluster should present slope changes with distance to the center, being flatter in the central parts than in the outer regions.

Examples of advanced dynamical evolution in star clusters have been reported in recent years, e.g. in NGC 3680 (Anthony-Twarog et al. 1991; Bonatto et al. 2004b) and M 67 (Bonatto & Bica 2003), in which the presence of a core depleted of low-MS stars and a halo rich in low-mass stars have been confirmed with 2MASS photometry.

The accurate determination of LF spatial variations, as well as the characterization of a cluster's stellar content, depends critically on a proper background subtraction. The uniform and essentially complete sky coverage provided by 2MASS (Two Micron All Sky Survey, Skrutskie et al. 1997) has proven to be a powerful tool for properly taking into account background regions with suitable star count statistics (see, e.g. Bonatto et al. 2004b; Bonatto & Bica 2003; Bica et al. 2003, 2004).

In the present work we investigate the dynamical state and stellar content of NGC 188. We employ J and H 2MASS photometry to analyse a large spatial area in the direction of the cluster. In particular, we search for spatial changes in the LF which would characterize the advanced dynamical state of this open cluster. This is the first analysis of NGC 188 in the near-infrared with wide spatial coverage and resolution.

This paper is organized as follows. In Sect. 2 we provide general data on NGC 188 and present a brief review on this open cluster. In Sect. 3 we obtain the 2MASS photometry and introduce the $J \times (J-H)$ colour−magnitude diagrams (CMDs). In Sect. 4 we discuss the projected radial density distribution of stars and derive structural parameters for NGC 188. In Sect. 5 we fit isochrones to the near-infrared CMD and derive cluster parameters. In Sect. 6 we derive the LFs and MFs, estimate the stellar mass still present in NGC 188 and examine the presence of unresolved binaries in the CMD. Concluding remarks are given in Sect. 7. In Appendix A we discuss the consequences of applying colour-filters to the CMD and the background subtraction.

2. The old open cluster NGC 188

NGC 188 has been in the spotlight since the early works of Sandage (1961, 1962) when the age of this open cluster was estimated to be $\tau_{\rm age} \sim 10-16$ Gyr, making NGC 188 the probably oldest observable open cluster in the Galaxy. However, later works revised its age downwards (see Carraro et al. 1994, for a comprehensive age census) to the presently accepted value of around 6–7 Gyr (von Hippel & Sarajedini 1998; Sarajedini et al. 1999). The WEBDA open cluster database[1] (Mermilliod 1996) gives $\tau_{\rm age} \approx 4.3$ Gyr for NGC 188.

[1] http://obswww.unige.ch/webda

The actual, advanced age of NGC 188 still makes it one of the oldest surviving open clusters in the Milky Way. As such, NGC 188 has been used to test stellar evolution models, since its CMD exhibits a wide giant branch (e.g. Twarog 1997; Norris & Smith 1985), blue stragglers (e.g. Leonard & Linnell 1992; Dinescu et al. 1996) and numerous binaries (von Hippel & Sarajedini 1998, and references therein). Most of the previous research has been restricted to optical bands.

One of the reasons why NGC 188 has survived to such an advanced age may be its almost circular, highly inclined external ($9.5 \leq R(\mathrm{kpc}) \leq 11$) orbit, which avoids the inner disk regions for most of the time (a plot of the Galactic orbit of NGC 188 is shown in Fig. 1 of Carraro & Chiosi 1994). As a consequence of its orbit, the probability of significant dynamical interactions with giant molecular clouds becomes considerably reduced and thus, the rôle of internal processes in the dynamical evolution of NGC 188 increases in importance.

Based on V and I-band photometry of the central parts of NGC 188, (von Hippel & Sarajedini 1998), and *UBVRI* CCD photometry, Sarajedini et al. (1999), suggested that NGC 188 has a typical initial mass function. But, as a consequence of the advanced, i.e. mass-segregated dynamical state, the low-mass stars presently missing from the central parts are either in the cluster outskirts or have left the cluster (von Hippel & Sarajedini 1998).

WEBDA gives a slightly subsolar metallicity for NGC 188, which agrees with other values, e.g. $[\mathrm{Fe/H}] = 0.02 \pm 0.11$ (Caputo et al. 1990), $[\mathrm{Fe/H}] = -0.12 \pm 0.16$ (Hobbs et al. 1990) and $[\mathrm{Fe/H}] = -0.02$ (Twarog et al. 1997).

The central coordinates of NGC 188, precessed to J2000, are $\alpha = 00^{\rm h}47^{\rm m}53^{\rm s}$ and $\delta = +85°15'30''$, which convert to $\ell = 122.85°$ and $b = +22.39°$.

3. The 2MASS photometry

Despite having lost its title as the oldest Galactic open cluster, NGC 188 still deserves attention, since its age implies advanced stellar and dynamical evolution, and its location in the Galaxy favours deep observations, particularly in the infrared. We base the present analysis of NGC 188 essentially on J and H 2MASS[2] photometry. 2MASS photometric errors typically attain 0.10 mag at $J \approx 16.2$ and $H \approx 15.0$, see e.g. Soares & Bica (2002). The VizieR[3] tool has been used to extract stars in a circular area of 45′ radius centered on the coordinates given in Sect. 2. In order to maximize the statistical significance and representativeness of background star counts, we used the stars in the outermost annulus ($40' \leq R \leq 45'$) as offset field. See Appendix A for a discussion on background subtraction.

In Fig. 1 we show the $J \times (J-H)$ CMDs for NGC 188 (left panel) along with the corresponding (equal area) offset field (right panel). In order to maximize visualization of star sequences, the CMD in the direction of NGC 188 has been built with stars extracted within an area of 15′ in radius.

[2] All Sky data release, available at
http://www.ipac.caltech.edu/2mass/releases/allsky/

[3] http://vizier.u-strasbg.fr/viz-bin/VizieR?-source=II/246

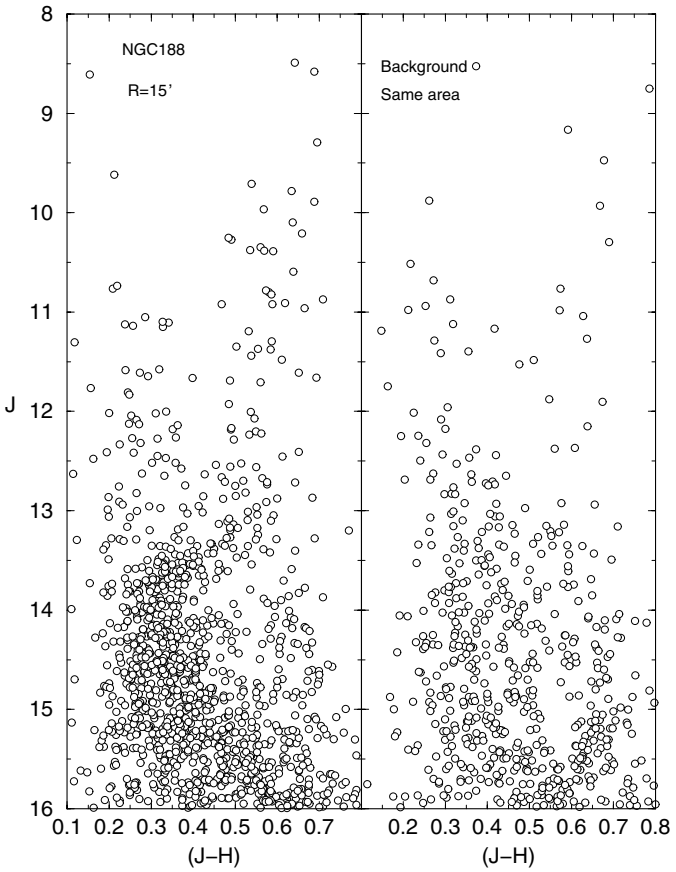

Fig. 1. $J \times (J-H)$ CMDs for the cluster NGC 188 (*left panel*, containing 1804 stars) and corresponding offset field (*right panel*, containing 998 stars). Both CMDs have been extracted within equal areas.

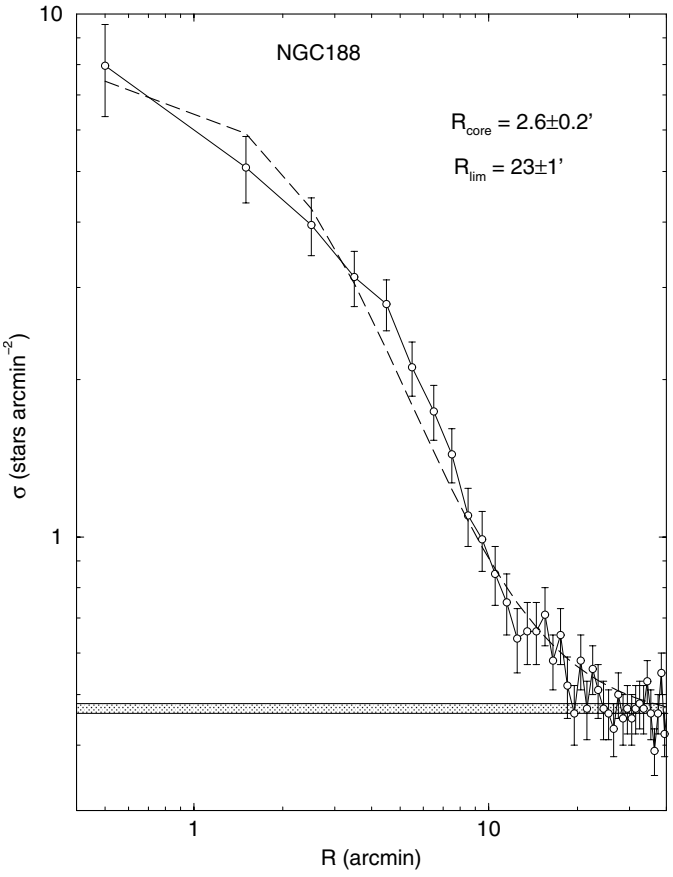

Fig. 2. Projected radial distribution of surface star density. The average background level is shown as a narrow shaded area; 1σ Poisson errors are also shown. Magnitude ($J < 16.0$) and colour cutoffs have been applied to the object and offset field. The dashed line shows a surface density profile (two-parameter King model) fit to the radial distribution of stars.

This dimension is, however, smaller than the limiting radius of NGC 188 (Sect. 4).

The near-infrared CMD of NGC 188 presents a well-defined MS with several stars occupying the turnoff, as well as a wide giant branch. The large width of the MS, which cannot be entirely accounted for by photometric errors (Sect. 6.3.1), indicates that this cluster may contain a large fraction of binaries, confirming previous optical observations (von Hippel & Sarajedini 1998, and references therein). These features are not present in the CMD of the comparison field. The nearly vertical sequence at $0.2 \leq (J-H) \leq 0.4$ and $10.5 \leq J \leq 13.5$, present in both CMDs but more populated in NGC 188, is probably due to disk stars and, to some extent, to the presence of blue stragglers in NGC 188 (Leonard & Linnell 1992; Dinescu et al. 1996).

The number of stars in the CMD in the direction of NGC 188 is 1804, while in its comparison field this number drops to 998.

4. Cluster structure

The overall cluster structure is analysed by means of the star density radial distribution, defined as the projected number of stars per area in the direction of a cluster, shown in Fig. 2 for NGC 188.

Before counting stars, we applied a cutoff ($J < 16.0$) to both cluster and offset field to avoid oversampling, i.e. spatial variations in the number of faint stars and spurious detections. Colour filters (Appendix A) have also been applied to both cluster and corresponding offset field, in order to account for the contamination by the Galaxy. This procedure has been previously applied in the analysis of the open cluster M 67 (Bonatto & Bica 2003). As a result of the filtering process, the number of stars in the direction of NGC 188 inside an area of $20'$ in radius turns out to be 1201, compared to 583 in its offset field (same area). The radial distribution has been determined by counting stars inside concentric annuli with a step of $1.0'$ in radius. The background contribution level corresponds to the average number of stars included in the external annulus, which lies outside the cluster border at $40' \leq R \leq 45'$.

The projected radial density profile of NGC 188 is very smooth with a well-defined central concentration of stars. The relatively large number of stars in this cluster produces small 1σ Poisson error bars along most of the profile. Considering the profile fluctuations with respect to the background level, we can define for NGC 188 a limiting radius of $R_{\rm lim} = 24 \pm 1'$. Because of the essentially null-contrast between cluster and background star density, any statistical analysis for regions

beyond $R_{\rm lim}$ would produce excessively high Poisson error bars, and, consequently, meaningless results. Thus, for practical purposes, we can consider that most of the cluster's stars are contained within $R_{\rm lim}$.

First order structural parameters of NGC 188 are derived by fitting the two-parameter King (1966a) surface density profile to the background-subtracted radial distribution of stars. The two-parameter King model essentially describes the central region of normal clusters (King 1966b; Trager et al. 1995). The fit has been performed using a non-linear least-squares fit routine which uses the error bars as weights. The best-fit solution is shown in Fig. 2 as a dashed line, and the resulting core radius is $R_{\rm core} = 2.6 \pm 0.2'$. With a distance to the Sun $d_\odot = 1.66 \pm 0.08$ kpc (Sect. 5), the linear core radius of NGC 188 turns out to be $R_{\rm core} = 1.3 \pm 0.1$ pc and the angular diameter ($2 \times R_{\rm lim}$) of $48 \pm 2'$ converts to a linear limiting diameter of 23.2 ± 1.5 pc.

Within the errors, the observed density profile departs from the two-parameter King model in opposite senses, particularly for the regions $0.9 \leq R(') \leq 3.5$ and $3.5 \leq R(') \leq 8.6$ (Fig. 2). Considering the physical premises of the King model, these deviations may be a consequence of the non-virialized dynamical state and possibly, some degree of non-sphericity in the spatial shape of NGC 188.

The core radius of NGC 188 is very similar to that of the $\tau_{\rm age} = 3.2$ Gyr, relaxed open cluster M 67 ($R_{\rm core} = 1.2 \pm 0.1$ pc – Bonatto & Bica 2003). However, its limiting diameter is larger than that of M 67 (12.7 ± 0.6 pc), probably a consequence of NGC 188's older age, more advanced dynamical state and larger mass (Sect. 6.2).

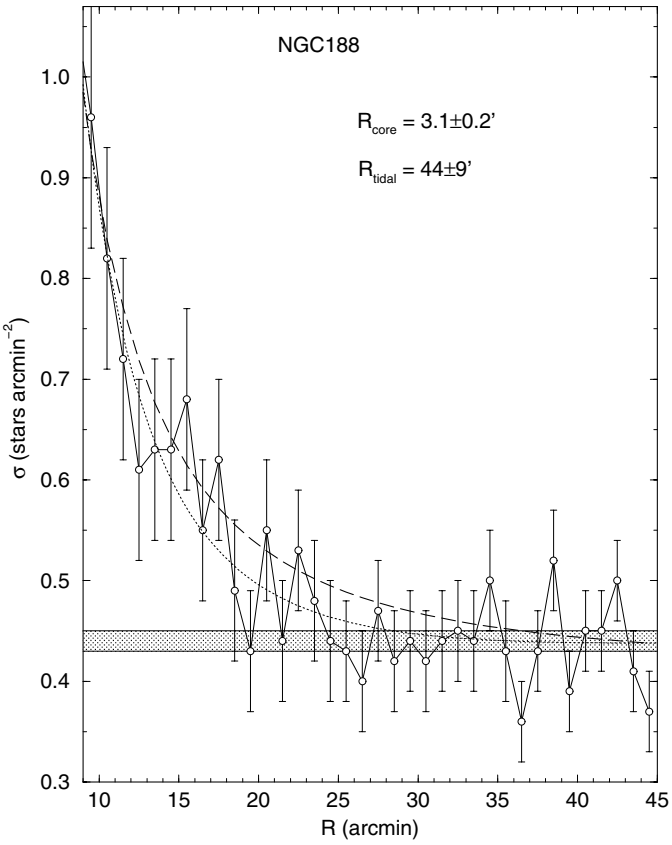

Fig. 3. Fit of King models to the projected radial distribution of stars of NGC 188. Dashed line: two-parameter model; dotted line: three-parameter model.

4.1. Tidal radius

The rather massive (Sect. 6.2) nature and present large galactocentric distance (Sect. 5) of NGC 188 make it possible to fit its projected radial distribution of stars with the more complete empirical density law of King (1962), which includes the tidal radius $R_{\rm tidal}$ as parameter in the model. The tidal radius depends both on the effect of the Galactic tidal field on the cluster and the subsequent internal relaxation and dynamical evolution of the cluster (Allen & Martos 1988). In particular, Oh & Lin (1992) have shown, through numerical simulations, that relaxation affects the tidal radius formation. In the case of NGC 188, the tidal radius determination is made possible by the spatial coverage and uniformity of 2MASS photometry, which allows one to obtain reliable data on the projected distribution of stars for large extensions around clusters.

The three-parameter model of King (1962) is a potential source of information both on the internal structure of the cluster, by providing reliable determinations of the core radius and the central density of stars, and on the Galactic tidal field, since the tidal radius is linked to the stripping of stars from the cluster by the Galactic tidal field. Since the three-parameter King model provides a better description of the outer regions of a cluster than the two-parameter model, it is particularly suitable for deriving a reliable value of $R_{\rm tidal}$.

The best-fit solution, with a correlation coefficient of 0.96 and an rms error of 0.83, resulted in $R_{\rm core} = 3.1 \pm 0.2'$ and $R_{\rm tidal} = 44 \pm 9'$, which convert to $R_{\rm core} = 1.5 \pm 0.1$ pc and $R_{\rm tidal} = 21 \pm 4$ pc. This solution is shown in Fig. 3 for regions more external than $R = 8'$. The two-parameter model fit is also shown in Fig. 3 for comparison purposes.

The present value of $R_{\rm tidal}$ is nearly twice as large as that estimated by Keenan et al. (1973) and, within the errors, comparable to the theoretical value calculated by Allen & Martos (1988). Interestingly, we note that the physical structure of NGC 188 extends well beyond the visual limits, since the presently derived value of $R_{\rm tidal}$ is about twice that of $R_{\rm lim}$. We note as well that the inclusion of the additional parameter $R_{\rm tidal}$ in the fit produced an increase of about 15% in $R_{\rm core}$, a value which differs $\approx 2\sigma$ from that derived with the two-parameter King model. However, since the two-parameter King model appears to give a better description of the inner regions of star clusters (King 1966b; Trager et al. 1995), we will adopt the previous value of $R_{\rm core} = 1.3 \pm 0.1$ pc as the core radius of NGC 188. With the values derived from the three-parameter model, the concentration parameter of NGC 188 turns out to be $c = \log\left(\frac{R_{\rm tidal}}{R_{\rm core}}\right) = 1.2 \pm 0.1$. To check how NGC 188 fits in the context of evolved star clusters, we compare its concentration parameter with those of 141 Galactic globular clusters

(compiled by Harris 1996)[4], which also includes the globular cluster sample of Trager et al. (1995). We conclude that NGC 188 is structurally comparable to the loose globular clusters, but still more concentrated than ≈25% of the sample.

5. Fundamental parameters

To maximize cluster membership probability, the analyses in the following two sections will be restricted to stars extracted within $R_{\rm lim}$ (Sect. 4). Cluster parameters will be derived using solar metallicity Padova isochrones from Girardi et al. (2002) computed with the 2MASS J, H, and $K_{\rm S}$ filters[5]. The 2MASS transmission filters produced isochrones very similar to the Johnson ones, with differences of at most 0.01 in $(J-H)$ (Bonatto et al. 2004a). The solar metallicity isochrones have been selected to be consistent with previous results (e.g. Caputo et al. 1990; Hobbs et al. 1990; and Twarog et al. 1997). For reddening and absorption transformations we use $R_{\rm V} = 3.2$, and the relations $A_{\rm J} = 0.276 \times A_{\rm V}$ and $E(J-H) = 0.33 \times E(B-V)$, according to Dutra et al. (2002) and references therein.

The presence of a well-defined turnoff and giant branch in the $M_J \times (J-H)$ CMD of NGC 188 constrain the age solution to the 6.3 Gyr, 7.1 Gyr and 8.0 Gyr Padova isochrones. The best fit, shown in Fig. 4, corresponds to the $\tau_{\rm age} = 7.1$ Gyr solution. Accordingly, we adopt as the age of NGC 188 $\tau_{\rm age} = 7.0 \pm 1.0$ Gyr. The M_J values are obtained after applying the distance modulus derived below for NGC 188. From the isochrone fit and related uncertainties we derive a distance modulus $(m-M)_0 = 11.1 \pm 0.1$, $E(B-V) = 0.0$ and a distance to the Sun $d_\odot = 1.66 \pm 0.08$ kpc. For illustrative purposes, we indicate representative stellar masses along the isochrone.

With the above distance to the Sun, the Galactocentric distance of NGC 188 is $d_{\rm GC} = 8.9 \pm 0.1$ kpc.

At this point it may be useful to estimate the expected mass of NGC 188 based on its Galactocentric distance and tidal radius. For clusters with a nearly circular orbit we can use the relation $M_{\rm c} \approx 3 M_{\rm G} \left(\frac{R_{\rm tidal}}{R_{\rm p}}\right)^3$ (King 1962), where $R_{\rm p}$ is the perigalacticon distance and $M_{\rm G}$ is the Galaxy mass inside $R_{\rm p}$. For the nearly circular orbit of NGC 188, $R_{\rm p} \approx d_{\rm GC}$, and at this distance, $M_{\rm G} \approx 1 \times 10^{11}\, M_\odot$ (Carraro & Chiosi 1994). With these values, the expected mass of NGC 188 turns out to be $M_{\rm c} \approx (3.9 \pm 2.2) \times 10^3\, M_\odot$.

6. Luminosity and mass functions

In this section we analyze the spatial dependence of the luminosity and mass functions in NGC 188, which will be subsequently used to derive the stellar mass still locked in this old open cluster.

6.1. Luminosity function

The 2MASS uniform sky coverage has been shown to be an ideal tool for studies like the present one, since the entire cluster area can be included in the analyses, and representative offset fields can be selected around the cluster (e.g. Bonatto & Bica 2003; Bica et al. 2003). As a consequence, advanced stages of mass segregation and the cumulative effects of the Galactic tidal pull can be properly detected and interpreted.

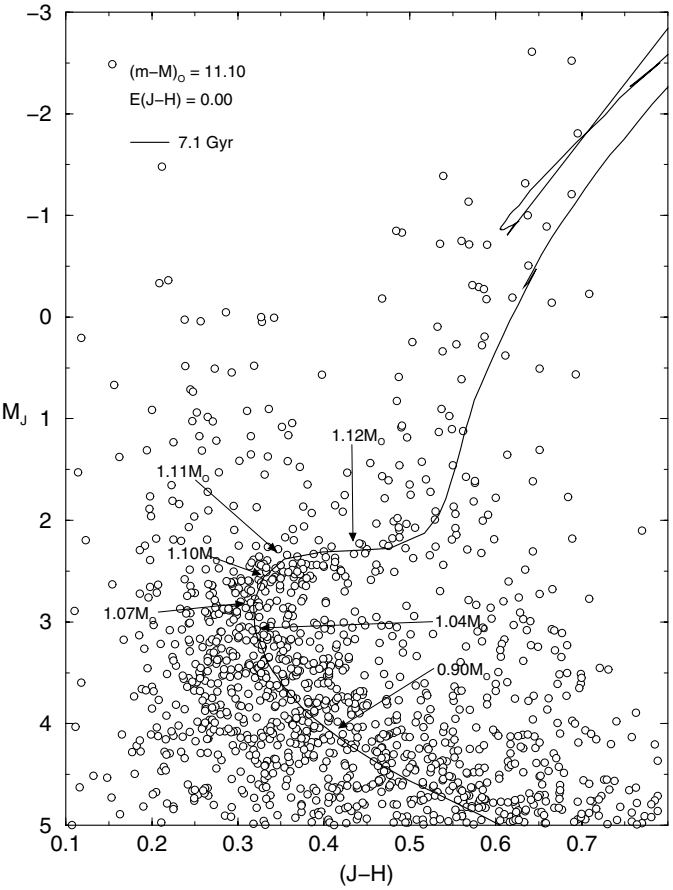

Fig. 4. Isochrone fit to the $M_J \times (J-H)$ CMD of NGC 188 with the $\tau_{\rm age} = 7.1$ Gyr Padova isochrone, resulting in $(m-M)_0 = 11.1 \pm 0.1$, $E(B-V) = 0.0$ and $d_\odot = 1.66 \pm 0.08$ kpc. Representative stellar masses are indicated.

In Fig. 5 we show the LFs ($\phi(M_J)$) in the J filter (shaded area), built as the difference in the number of stars in a given magnitude bin between object (continuous line) and offset field (dotted line). The LFs are given in terms of the absolute magnitude M_J, obtained after applying the distance modulus derived in Sect. 5. The bin in magnitude is $\Delta M_J = 0.25$ mag. The LFs in Fig. 5 are built after applying magnitude ($J < 16.0$) and colour cutoffs to the object and offset field (Sect. 5).

The large projected area of NGC 188, containing ~620 member stars (Sect. 4), can be used to search for spatial variations in the stellar content, with statistically significant results. Thus, LFs for different regions inside NGC 188 have been built following the structures present in the radial density profile (Fig. 2). These LFs are shown in panels (a) to (d) of Fig. 5. In particular, the LF in panel (c) corresponds to the core region, while in panel (b) we show the overall ($0.0' \le R \le R_{\rm lim}$) LF. The background $\phi(M_J)$ has been scaled to match the projected area of each region. Representative MS spectral types (adapted from Binney & Merrifield 1998)

[4] http://physwww.physics.mcmaster.ca/%7Eharris/mwgc.dat

[5] Available at http://pleiadi.pd.astro.it

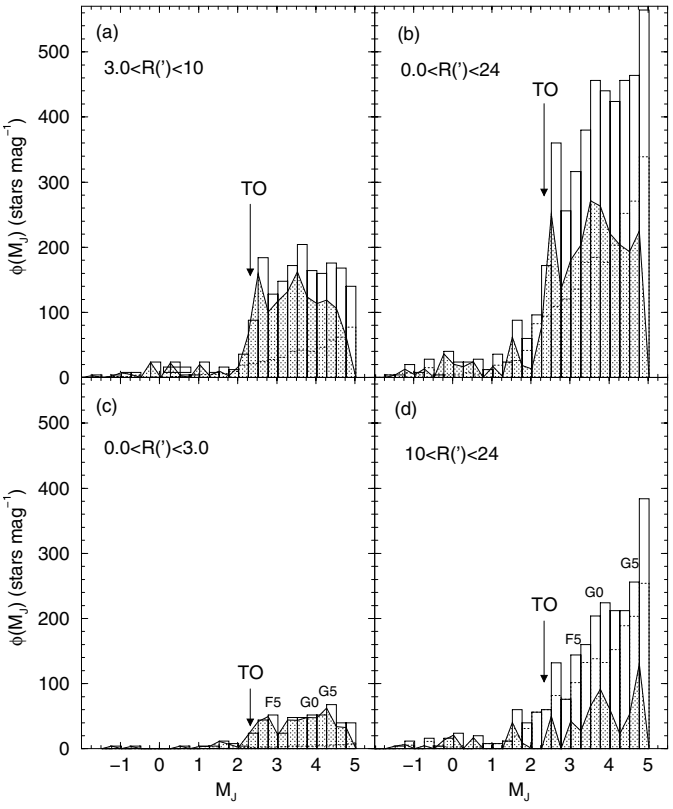

Fig. 5. Luminosity functions ($\phi(M_J)$) in terms of the absolute magnitude M_J. Magnitude ($J < 16.0$) and colour cutoffs have been applied to the object and offset fields. Continuous line: star counts in the cluster area; dotted line: star counts in the offset field; shaded area: background-subtracted LF. The turnoff (TO) is indicated in each panel.

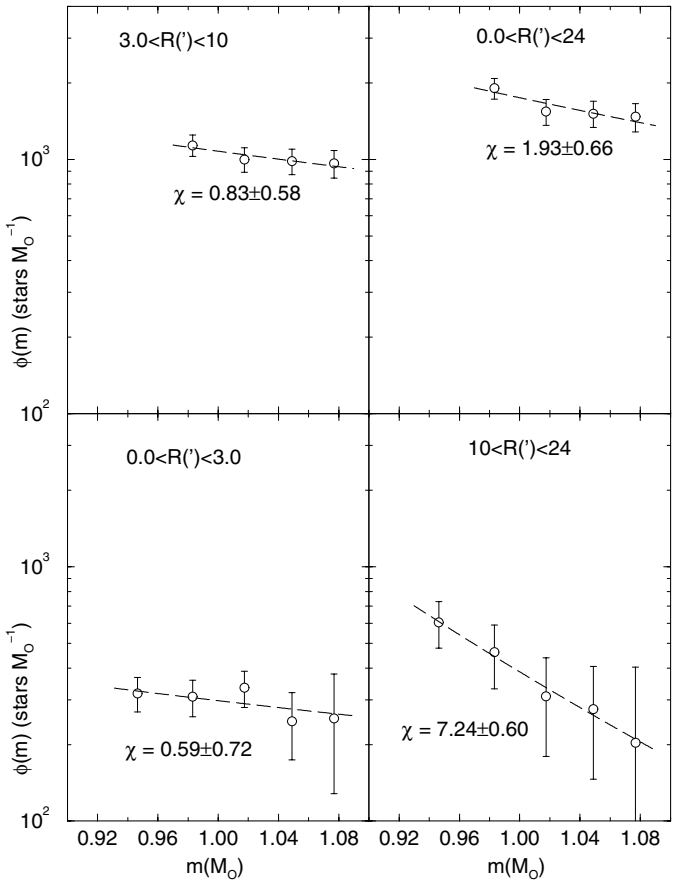

Fig. 6. Mass functions $\phi(m)$ restricted to the turnoff–turnover region. The MF fits $\phi(m) \propto m^{-(1+\chi)}$ are shown as dashed lines.

are shown in panels (c) and (d). The turnoff ($M_J \approx 2.27$, spectral type ≈F 3, mass ≈ 1.10 $M_\odot$) is indicated in all panels. The excess at $M_J \approx 2.5$ corresponds to the accumulation of stars near the turnoff (Fig. 4). Hereafter we will refer to the maximum number count in the LFs as turnover.

As expected from the long-term dynamical evolution of this old open cluster, the large number of member stars contained inside $R = 24'$ (panels (a), (c) and (d)), does not present a uniform spatial distribution of MS spectral types (magnitude range $3.0 \leq M_J \leq 4.5$). The region with $R \geq 10'$ seems to have an LF steeper than those of the more internal ones, the core region in particular, which is characteristic of mass segregation.

6.2. Mass function

Cluster mass estimates can be made after converting the turnoff–turnover LFs into MFs according to $\phi(m) = \phi(M_J)\left|\frac{\mathrm{d}m}{\mathrm{d}M_J}\right|^{-1}$, using the stellar mass-luminosity relation taken from the 7.1 Gyr Padova isochrone. To avoid the star excess near the turnoff, we restricted this analysis to stars with mass ≤ 1.08 $M_\odot$ ($M_J \approx 2.7$). To increase the statistical representativeness of our results, we applied this method to the core region, $3.0' \leq R \leq 10'$, $10' \leq R \leq 24'$ and to the overall LF. The resulting MFs, including 1σ Poisson error bars for each data point, are shown in Fig. 6.

The spatial variation in the stellar content of NGC 188 is clearly seen in the MFs shown in Fig. 6, being flat in the core region and very steep in the region $10' \leq R \leq 24'$. We quantify this effect by fitting the function $\phi(m) \propto m^{-(1+\chi)}$ to the MFs, using a weighted non-linear least-squares routine. The results are given in Table 1. The number of stars from the high-mass end to just below the turnoff ($m = 1.08\,M_\odot$) is obtained by numerical integration of the LFs in the corresponding mass interval (Col. 4). Then, multiplying this number by the mass at the turnoff gives us an estimate of the mass stored in evolved stars ($m^*_{\rm evol}$), which is listed in Col. 3 of Table 1. In Col. 6 we provide the MS mass, obtained by numerical integration of the MFs from the turnover to $m = 1.08\,M_\odot$. Column 7 gives the total observed mass contained in each sampled region of NGC 188, while the corresponding number of observed stars is listed in Col. 8. In Col. 9 we provide an estimate of the observed mass density in each region. Uncertainties in the values of χ (Col. 5) are derived from the least-squares fit, and uncertainties in the mass and number of stars come from error propagation.

The advanced, mass-segregated dynamical state of NGC 188 is reflected particularly in the flat MF slope in the core region ($\chi = 0.6 \pm 0.7$) compared to the very steep slope ($\chi = 7.2 \pm 0.6$) in the region $10' \leq R \leq 24'$. Indeed, the mass segregation is fully characterized by the positive gradient, with respect to the distance to the cluster center, presented by the MF slopes (Table 1).

Table 1. Mass-function fit and related parameters.

						Observed			Extrapolated		
Region		$m^*_{\rm evol}$	Fit	χ	$m_{\rm MS}$	m	N	$\rho*$	m	N	$\rho*$
(′)	(pc)	($M_\odot$)	($M_\odot$)		($M_\odot$)	($M_\odot$)	(stars)	($M_\odot\,{\rm pc}^{-3}$)	($M_\odot$)	(stars)	($M_\odot\,{\rm pc}^{-3}$)
(1)	(2)	(3)	(4)	(5)	(6)	(7)	(8)	(9)	(10)	(11)	(12)
Core	0.0–1.4	35	0.95 → 1.08	0.6 ± 0.7	38 ± 3	73 ± 3	69 ± 5	6.7	609 ± 261	2070 ± 1470	55.5 ± 23.8
3.0–10	1.4–4.8	109	0.98 → 1.08	0.8 ± 0.6	105 ± 34	213 ± 7	200 ± 5	0.5	2260 ± 968	7700 ± 5440	5.2 ± 2.2
10–24	4.8–11.6	49	0.95 → 1.08	7.2 ± 0.6	47 ± 2	94 ± 3	91 ± 4	0.02	1090 ± 475	3760 ± 2670	0.2 ± 0.1
Overall	0.0–11.6	193	0.98 → 1.08	1.9 ± 0.7	187 ± 12	380 ± 12	333 ± 76	0.1	3760 ± 1610	12800 ± 9040	0.6 ± 0.3

Notes. Column 1: spatial region expressed in arcmin; Col. 2: same as Col. 1 in pc; Col. 3: mass of stars later than the turnoff; Col. 4: mass range to which the MF has been fitted; Col. 5: MF slope; Col. 6: turnoff–turnover mass calculated from the MF fit; Col. 7: observed mass, sum of $m^*_{\rm evol}$ and $m_{\rm MS}$; Col. 8: number of observed stars; Col. 9: observed mass density; Col. 10: extrapolated mass; Col. 11: extrapolated number of stars; Col. 12: extrapolated mass density.

At this point it may be interesting to compare the dynamical mass of NGC 188 (Sect. 5) with an independent determination of the mass still locked up in stars in this cluster by directly extrapolating the derived MF down to the theoretical stellar low-mass end $m_{\rm low} = 0.08\,M_\odot$. Thus, according to the MF in Table 1, the total stellar mass in NGC 188 is $m_{\rm tot} \sim (1.8 \pm 0.7) \times 10^4\,M_\odot$. On the other hand, Kroupa et al. (1991) and Kroupa (2001) presented evidence that the MFs of most globular and open clusters flatten below $\sim$0.5 $M_\odot$. As a consequence, the total stellar mass in NGC 188 is probably less than the value derived above, since most of the stars are expected to be found in the low-mass range. Accordingly, we derive a more conservative total mass value for NGC 188 assuming the universal IMF of Kroupa (2001), in which $\chi = 0.3 \pm 0.5$ for 0.08 $M_\odot$–0.50 $M_\odot$, and $\chi = 1.3 \pm 0.3$ for 0.50 $M_\odot$–0.98 $M_\odot$. For 0.98 $M_\odot$–1.08 $M_\odot$ we adopt the value derived in this paper, $\chi = 1.93 \pm 0.66$. As expected, the resulting total stellar mass drops to $m_{\rm tot} \sim (3.8 \pm 1.6) \times 10^3\,M_\odot$. This mass value is in close agreement with the mass estimated from NGC 188's galactocentric distance and tidal radius (Sect. 5). Following the procedure described above, we calculate for each region of NGC 188 the extrapolated mass, number of stars and corresponding mass density. These quantities are listed in Cols. 10–12 respectively of Table 1.

Mass segregation in a star cluster scales with the relaxation time, defined as $t_{\rm relax} = \frac{N}{8 \ln N} t_{\rm cross}$, where $t_{\rm cross} = R/\sigma_{\rm v}$ is the crossing time, N is the number of stars and $\sigma_{\rm v}$ is the velocity dispersion (Binney & Tremaine 1987). For NGC 188, $R \approx 11$ pc (Sect. 4), and we assume a typical $\sigma_{\rm v} \approx 3\,{\rm km\,s^{-1}}$ (Binney & Merrifield 1998). Thus, for the observed number of stars, $t_{\rm relax} \sim 24$ Myr, and for the extrapolated number of stars, $t_{\rm relax} \sim 600$ Myr. Both estimates of $t_{\rm relax}$ are much smaller than the age of NGC 188, which is consistent with the presence of mass segregation. Interestingly, the first estimate of $t_{\rm relax}$ in NGC 188 was made by van den Bergh & Sher (1960) who from star counts derived a mass of $\sim$900 $M_\odot$ and a radius of $\sim$6.5′, thus resulting in $t_{\rm relax} \sim 64$ Myr.

With an age of about 7 Gyr, NGC 188 must have lost a significant fraction of its primordial mass through (i) internal processes, such as mass loss and disruption through the evolution of massive stars in the early phases, and evaporation along the cluster's evolution; and (ii) external processes such as tidal shocks in the Galactic disk and encounters with giant molecular clouds. During the first few million years of a massive cluster's life, as the primordial gas is removed from the system, the gravitational well changes, decreasing the escape velocity. As a consequence, the high-velocity stars can be ejected from the cluster in a fraction depending on the initial cluster configuration, star formation efficiency and velocity distribution of the stars (Adams 2000; de la Fuente Marcos & de la Fuente Marcos 2002). Subsequently, evaporation sets in and starts reducing the cluster mass. Examples of population decline with cluster age, against evaporation, can be seen in the numerical models (including stellar mass loss) of de la Fuente Marcos & de la Fuente Marcos (2002). Disk shocking plays an important rôle not only in reducing a cluster's mass but also in flattening its spatial shape. Indeed, Bergond et al. (2001) estimate an upper limit of 5–10% for the mass-loss efficiency during a single disk crossing, and observe strong flattening in the shapes of NGC 2287 and NGC 2548, which they attribute to disk shocking.

With respect to NGC 188, the present-day number of stars of $\sim 10^4$ (Table 1) is already larger than the primordial number of stars in the most-populous models available in de la Fuente Marcos & de la Fuente Marcos (2002). Consequently, taking into account (i) the sharp population decline with time observed in the populous models of de la Fuente Marcos & de la Fuente Marcos (2002); (ii) the other mass-reducing processes discussed in the preceding paragraph; and (iii) the old age derived for NGC 188 ($\approx$7 Gyr), it is clear that the primordial population of stars in NGC 188 must have significantly exceeded 10^4 stars. Consequently, its primordial mass must have been larger than $4 \times 10^3\,M_\odot$.

6.3. Binaries in NGC 188

The results presented in Sects. 6.1 and 6.2 are based on the simple assumption that all stars in the CMD are single objects.

However, stars in multiple systems, binaries in particular, usually account for a considerable fraction of the stellar content in open clusters (e.g. Montgomery et al. 1993).

As a consequence of the dynamical evolution in open clusters, multiple systems tend to concentrate in the central regions, thus changing the initial spatial distribution of stars (Takahasi & Portegies Zwart 2000). Observationally, the main effect of a significant fraction of unresolved binaries in the central parts of a star cluster is that the number of low-mass stars is underestimated with respect to the higher-mass stars. Thus, the observed central LF (or MF) turns out to be flatter than that of the actual, resolved stellar distribution. In addition, the resulting MF changes will depend both on the binary fraction and MS mass range (e.g. Kroupa et al. 1991, and references therein).

With respect to NGC 188, von Hippel & Sarajedini (1998) estimate a fraction of ≈50% of multiple systems in the central region. At this point, the natural question to ask is whether this large fraction of binaries in NGC 188 may account for the observed flat central MF (Fig. 6 and Table 1).

To address this question we adopted the following approach. First we generate a population of single stars according to a standard ($\chi = 1.35$) Salpeter MF distribution. To be consistent with the 2MASS CMD of NGC 188, we used single stars in the mass range $0.15-1.10\,M_{\odot}$. Then, according to a pre-defined fraction of CMD binaries, we randomly select stars from the original distribution and build the specified number of binaries. Mass and luminosity biases are avoided in this process (Kroupa 2002; Mazeh et al. 2003) and consequently, the probability of a star being selected as a binary member depends only on the number frequency of its mass. Each star selected to become a binary member is subsequently deleted from the original population. Based on the 7.1 Gyr isochrone mass-luminosity relation, the combined luminosity of each pair member is converted back to mass. When all binaries are thus formed and their masses stored in the new population distribution, we add the remaining (not-paired) original single stars to the final population distribution. The final, observed MF is then built by counting the combined number of single and paired stars in each mass bin. To reach a high level of statistical significance, the initial single-star distribution contains 10^6 stars.

To check how a varying binary population may affect the original, single-star MF, we applied the above approach to MFs with slopes $\chi_{\rm imf} = 1.0, 1.5$ and 2.0, and for fractions of CMD binaries $f_{\rm bin} = 0.5, 0.75$ and 1.0. $f_{\rm bin} = 0.75$ means that 75% of the observed CMD objects are binaries. We illustrate this effect for $\chi_{\rm imf} = 1.0$ in the top panel of Fig. 7, in which the heavy solid line represents the MF of the single-star distribution. The final MF distributions are shown as dotted, thin solid and dashed lines, respectively for the binary fractions $f_{\rm bin} = 0.5, 0.75$ and 1.0. All MFs in Fig. 7 are scaled so that the total number of stars produced by each MF ($\int \phi(m)\,{\rm d}m$) is the same.

Since most of the single-star distribution is made up of low-mass stars, binary formation severely depletes the original MF, particularly for $m \leq 0.25\,M_{\odot}$. The binaries thus formed have a mass ratio $q \sim 0.65$ and tend to accumulate, in varying proportions (according to $f_{\rm bin}$ and $\chi_{\rm imf}$), in the region $0.3 \leq m(M_{\odot}) \leq 0.9$ of the observed MF. Thus, considering the distribution of stars with mass $\geq 0.25\,M_{\odot}$, the final MFs indeed turn out flatter than the single-star distributions. However, for stars in the mass range from which we derived the present results (mass $\geq 0.8\,M_{\odot}$), the final distributions become even steeper than the original ones. This is particularly true for the $\chi_{\rm imf} = 2.0$ MF, since this distribution contains the largest fraction of low-mass stars.

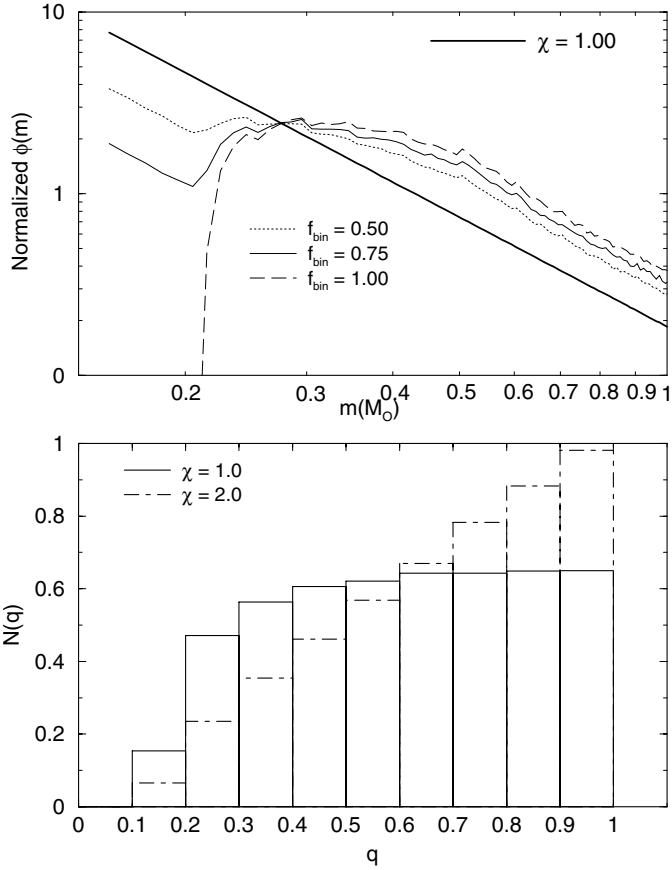

Fig. 7. *Top panel*: varying binary fractions are tested for a single-star MF of slope $\chi_{\rm imf} = 1.0$. The (original) single star population MF is represented by the heavy solid line. All MFs are scaled so that they produce the same total number of stars. *Bottom panel*: simulated mass-ratio ($q = M_2/M_1$) distribution for MFs with $\chi_{\rm imf} = 1.0$ and 2.0. The binary fraction for both distributions is $f_{\rm bin} = 0.75$.

Table 2. Binary effects on MFs.

		$f_{\rm bin} = 0.50$		$f_{\rm bin} = 0.75$		$f_{\rm bin} = 1.00$	
$\chi_{\rm imf}$	q	$\chi_{0.2-1.1}$	$\chi_{0.6-1.1}$	$\chi_{0.2-1.1}$	$\chi_{0.6-1.1}$	$\chi_{0.2-1.1}$	$\chi_{0.6-1.1}$
1.0	0.61 ± 0.23	0.50	1.12	0.36	1.14	0.26	1.15
1.5	0.65 ± 0.23	0.90	1.79	0.75	1.88	0.75	1.92
2.0	0.69 ± 0.22	1.37	2.33	1.25	2.43	1.29	2.50

Notes. $\chi_{\rm imf}$ is the original MF slope; $\chi_{0.2-1.1}$ is the MF slope in the mass range $0.2 \leq m(M_{\odot}) \leq 1.1$ and $\chi_{0.6-1.1}$ is the slope in the range $0.6 \leq m(M_{\odot}) \leq 1.1$.

We summarize the above discussion in Table 2, in which we give, for each $\chi_{\rm imf}$, the resulting slopes obtained from MF fits to the mass ranges $0.2 \leq m(M_\odot) \leq 1.1$ and $0.6 \leq m(M_\odot) \leq 1.1$.

As expected, the $0.2 \leq m(M_\odot) \leq 1.1$ MF flattening degree is largest for the flattest single-star MF, since the relative number of higher-mass stars with respect to lower-mass stars is favoured in this distribution. Indeed, the average binary mass ratio for $\chi_{\rm imf} = 1.00$ is, within the uncertainties, the smallest of the MFs tested here.

Because of the binary formation, the accumulation of stars in the observed MFs for mass $\leq 0.9\,M_\odot$ ends up increasing the MF slope in the $0.6 \leq m(M_\odot) \leq 1.1$ mass range. This effect is present for any $\chi_{\rm imf}$ and $f_{\rm bin}$.

Finally, we present in the bottom panel of Fig. 7 the mass-ratio ($q = M_2/M_1$) distribution obtained for MFs with $\chi_{\rm imf} = 1.0$ and 2.0, derived for stars with masses in the range $0.15-1.1\,M_\odot$. The binary fraction in both distributions shown in Fig. 7 is $f_{\rm bin} = 0.75$. Since the mass ratio depends only on the masses of the two companions, the distributions for different binary fractions are essentially the same, but vary with different MF slopes. Interestingly, the nearly-flat distribution for $\chi_{\rm imf} = 1.0$ for $0.3 < q < 1.0$ agrees with the results presented in Mazeh et al. (2003) for spectroscopic binaries with primary masses in the range $0.6-0.85\,M_\odot$. The similarity between the simulated mass-ratio distribution for $\chi_{\rm imf} = 1.0$ (Fig. 7) and that observed in spectroscopic binaries (Mazeh et al. 2003) suggests that Galactic field stars tend to have an MF with a slope around $\chi = 1$.

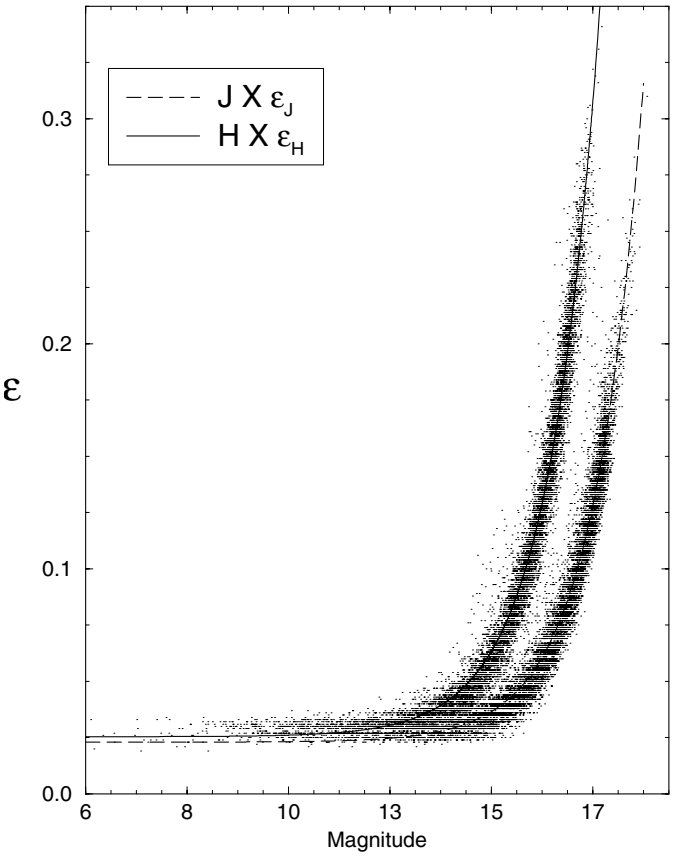

Fig. 8. Average photometric uncertainty related to a given magnitude. Solid line: $\epsilon_H \times H$; Dashed line: $\epsilon_J \times J$. Least-squares fits result in $\epsilon_H = 0.025 + 1.92 \times 10^{-8} e^{(H/0.998)}$ and $\epsilon_J = 0.023 + 4.78 \times 10^{-9} e^{(J/0.976)}$.

6.3.1. Widening of CMD sequences

In the magnitude range we are dealing with in this work, uncertainties in J and H are typically $\leq$0.10 mag (e.g. Soares & Bica 2002). Despite the small values, the uncertainties produce an additional scatter on the observed CMDs and, as a consequence, a widening, particularly of the MS. NGC 188 indeed presents a wide MS (Figs. 1 and 4), and in this section we investigate how much of the MS width can be attributed to binaries and photometric errors. The approach here is to produce synthetic CMDs which simulate both effects and to compare them with actual CMDs of NGC 188.

In 2MASS photometry, the average photometric uncertainty (ϵ) for a given magnitude follows a tight relation with magnitude, as can be seen in Fig. 8, in which we plot data for NGC 188. For each J magnitude, the photometric error is obtained by randomly selecting a value in the interval $(-\epsilon_J \leq \epsilon \leq +\epsilon_J)$, assuming that ϵ follows a normal distribution curve. H errors are obtained similarly.

We first generate an MS stellar distribution according to a given initial mass function (IMF) and binary fraction, as described in Sect. 6.3. For NGC 188, the MS is assumed to follow the 7.1 Gyr isochrone. For each single-mass star and binary thus formed, uncertainties are assigned to the J and H magnitudes as described above. Finally, we add to the simulated CMD a background stellar distribution.

We test this approach by comparing the resulting CMDs with the observed one for $R \leq 10'$, shown in panel (d) of Fig. 9; the corresponding (same area) background field is shown in panel (a). To be consistent with the results of Sects. 6.2 and 6.3, we use an IMF with $\chi = 0.8$ and binary fraction $f_{\rm bin} = 0.50$. In addition, the simulated MSs have been generated with approximately the same number of stars as the observed, background-subtracted MS. We illustrate the individual scatter produced in the IMF distribution by the photometric errors and binaries, respectively in panels (b) and (c). The MSs in panels (b) and (c) have similar widths, although, as expected, the photometric errors produce scatter symmetrically distributed about the isochrone. The binaries, as expected, produce scatter biased towards brighter magnitudes. This effect was originally pointed out by Kuiper (1935). Finally, assigning photometric errors to the binaries and single stars of panel (c), and adding the offset field (panel (a)), we obtain the comparison CMDs in panels (e) and (f). For illustrative purposes, the 7.1 Gyr isochrone is included in all panels.

The present approach produced near-IR CMD sequence widenings similar to those obtained in the optical by, e.g. Kerber et al. (2002), Hernandez et al. (1999) and Hurley & Tout (1998), in which binaries and photometric errors are also included in CMD statistical simulations.

The scatter resulting from the combination of binaries ($f_{\rm bin} = 0.50$) and photometric errors (panel (f)) produces a thick MS which, in general terms, presents similarities with the

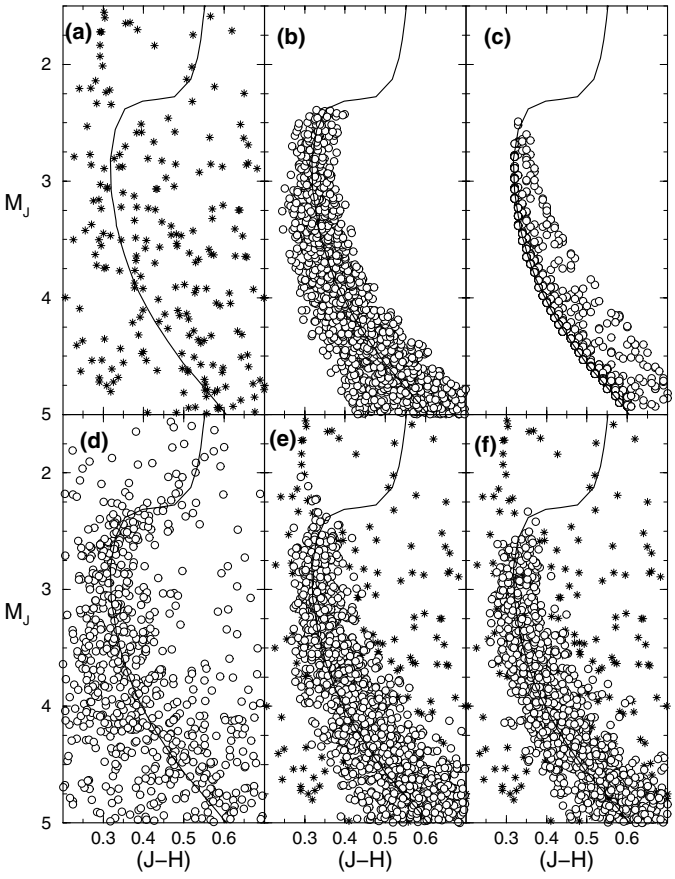

Fig. 9. Simulated CMDs compared to the observed one. Panel **a)** offset field; **b)** scatter produced by 2MASS photometric errors only on a $\chi = 0.8$ IMF distribution; **c)** scatter produced by a binary fraction $f_{\rm bin} = 0.5$ on the same IMF of panel **b)**; **d)** observed CMD in the region $R \leq 10'$; **e)** CMD resulting from the combination of photometric errors, binaries ($f_{\rm bin} = 1.0$) and the offset field; **f)** same as **e)** but for $f_{\rm bin} = 0.5$. The offset field distribution is shown by the stars.

observed MS (panel (d)). However, the observed MS is clearly wider than the simulated one. Since the photometric errors are indeed very small in the MS magnitude range of NGC 188, the observed excess width is probably due to a larger binary fraction. Indeed, a better representation of the observed MS is obtained with $f_{\rm bin} = 1.0$ (panel (e)). Interestingly, Kroupa et al. (1991) found that for stars to about 100 pc from the Sun, the LFs determined both from photometric parallax and counting individual stars are consistent with each other if all stars are in binary systems.

In conclusion, the above arguments show that the presence of unresolved binaries in the CMD, even in large fractions, cannot account for the large MF flattening degree detected in the central parts of NGC 188. On the other hand, the width of the observed MS can be mostly accounted for by a binary population with a fraction $f_{\rm bin} \approx 1.0$, provided that photometric errors are properly taken into account.

7. Concluding remarks

In the present work, the physical structure, stellar content and dynamical state of the old open cluster NGC 188 have been analysed. The spatial dependences of the luminosity and mass functions were studied in detail. The present analyses made use of J and H 2MASS All Sky data release photometry.

NGC 188 is about 7 Gyr old and has survived past the age at which most open clusters have already dissolved, possibly leaving behind a cluster remnant (Carraro 2002; Pavani et al. 2002, 2003). One of the reasons for such a long life may be the orbit of NGC 188, which avoids the inner disk regions most of the time, thus decreasing the probability of large-scale encounters with giant molecular clouds. The large Galactocentric distance of NGC 188, $d_{\rm GC} \approx 8.9$ kpc, also accounts for the long-time survival of this open cluster, together with its relatively large mass.

NGC 188 presents a smooth radial distribution of stars (Sect. 4), with small 1σ Poisson error bars because of the large number of member stars. Its projected radial density profile has a marked central concentration of stars (Fig. 2). From a two-parameter King model fit to the projected radial density profile we derive a core radius $R_{\rm core} = 1.3 \pm 0.1$ pc. The tidal radius, $R_{\rm tidal} = 21 \pm 4$ pc, has been derived by fitting a three-parameter King model to the profile. The tidal radius is nearly twice as large as the visually determined linear limiting radius of 11.6 ± 0.8 pc. The concentration parameter of NGC 188, $c = 1.2 \pm 0.1$, makes this open cluster structurally comparable to the loose globular clusters, but still more concentrated than ≈25% of them. The observed projected radial density profile of NGC 188 departs from the two-parameter King model in two inner regions, which reflects the non-virialized dynamical state (despite the cluster's old age) and possibly, some degree of non-sphericity in the spatial shape of this old open cluster. Its $M_J \times (J-H)$ CMD (Fig. 4), with a well-defined turnoff and giant branch, as well as evidence of blue stragglers and binaries, can be fitted with the 7.0 ± 1.0 Gyr solar metallicity Padova isochrones. The best-fit with the 7.1 Gyr isochrone and related uncertainties result in $(m-M)_0 = 11.1 \pm 0.1$, $E(B-V) = 0.0$ and $d_\odot = 1.66 \pm 0.08$ kpc.

Mass segregation in NGC 188 is reflected in the spatial variation of its MF (Fig. 7), which is flat ($\chi = 0.6 \pm 0.7$) in the core region and steep ($\chi = 7.2 \pm 0.6$) in the outskirts. The MF fit $\phi(m) \propto m^{-(1+\chi)}$ resulted in an observed stellar mass (MS and giants) of $\approx 380 \pm 12\, M_\odot$. If one extrapolates the 2MASS MF fit down to the theoretical low-mass end $m_{\rm low} = 0.08\, M_\odot$ the total stellar mass in NGC 188 turns out to be $\sim(1.8 \pm 0.7) \times 10^4\, M_\odot$. However, if we assume a more representative IMF, which flattens for masses below $\sim 0.5\, M_\odot$, the total stellar mass in NGC 188 turns out to be $\sim(3.8 \pm 1.6) \times 10^3\, M_\odot$. This value is in close agreement with the mass estimated for a tidally truncated cluster at the present position and with the same tidal radius as NGC 188. The primordial mass in NGC 188 must have been significantly larger than $\sim 4 \times 10^3\, M_\odot$, since mass-loss processes such as evaporation and tidal stripping have been acting on this cluster for about 7 Gyr.

We also addressed the observational consequences of the presence of unresolved binaries in the central parts

of NGC 188, since these systems may dominate the 2MASS CMD. After testing the effects of different binary fractions and single-star distributions, we conclude that unresolved binaries alone cannot account for the flatness of the central MF in NGC 188, thus supporting the mass-segregation scenario. Finally, the large width exhibited by the MS of NGC 188 cannot be explained only by photometric errors; instead, it is consistent with a binary fraction of nearly 100%.

Acknowledgements. We thank the referee for helpful suggestions. This publication makes use of data products from the Two Micron All Sky Survey, which is a joint project of the University of Massachusetts and the Infrared Processing and Analysis Center/California Institute of Technology, funded by the National Aeronautics and Space Administration and the National Science Foundation. We employed catalogues from CDS/Simbad (Strasbourg) and Digitized Sky Survey images from the Space Telescope Science Institute (US Government grant NAG W-2166) obtained using the extraction tool from CADC (Canada). We also made use of the WEBDA open cluster database. We acknowledge support from the Brazilian Institution CNPq.

Appendix A: Effects of colour filters and background selection

Since star clusters are usually projected against relatively rich Galactic fields, the observed CMDs may be heavily contaminated by background stars, which thus introduce additional noise in the photometry. This effect is particularly critical for objects projected against the Galactic disk or bulge. In this context, a careful subtraction of this contamination, usually by means of colour and magnitude filters, is necessary. In this section we will examine the consequences of having applied filters to the CMD of NGC 188, both in its physical structure and LF.

NGC 188 lies at $b = +22.39°$, consequently its CMD is not heavily contaminated, except for disk stars (nearly vertical sequence at $(J-H) \approx 0.2$–0.4) and the faint ones for $J \geq 16$. Thus, we used a colour filter which follows the 7.1 Gyr isochrone shape and preserves most of the stars. The filter is shown as a dashed line in Fig. A.1.

In Fig. A.2 (top panel) we compare the radial distribution of stars obtained with no filter (circles) and that using the colour filter (squares). The background level has been subtracted from both curves. The filtering effect, besides decreasing the number of stars, produces a thinner and smoother profile with respect to that without filter. Indeed, $R_{\rm core} = 2.62'$ for the filtered profile while $R_{\rm core} = 3.14'$ for the unfiltered one.

The overall ($0'$–$22'$) filtered and unfiltered LFs are shown in the bottom panel of Fig. A.2. The two curves are very similar from $J = 8$ to $J \approx 13.5$. As expected, the differences begin to increase for fainter magnitudes, in particular for $J \geq 14.5$, the magnitude range where most of the discarded stars are found. If these stars were preserved in the analysis, they would produce an abnormally steep profile which would artificially increase the number of low-mass stars in the cluster.

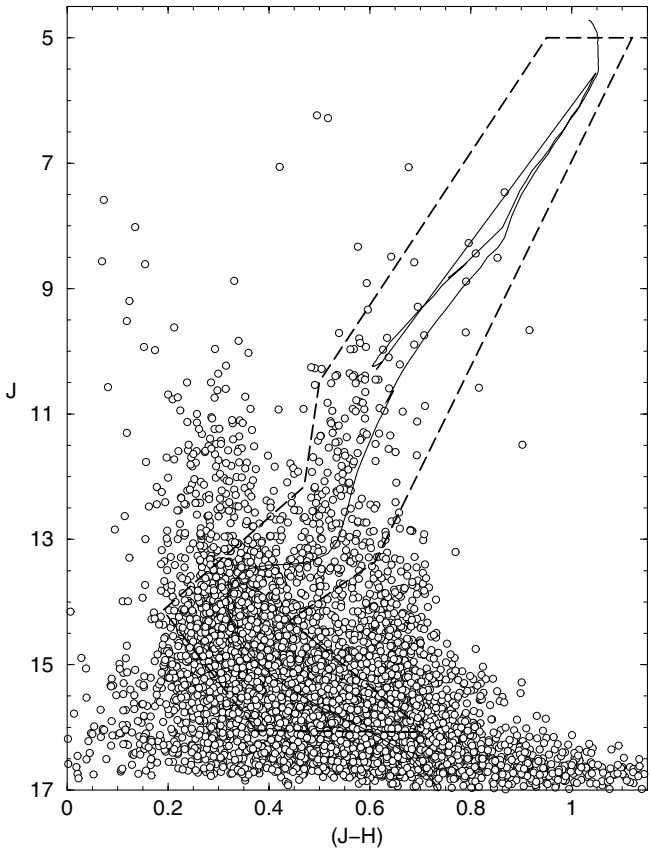

Fig. A.1. The dashed line shows the colour filter used for NGC 188. Magnitude cutoffs are $J = 5$ and $J = 16$.

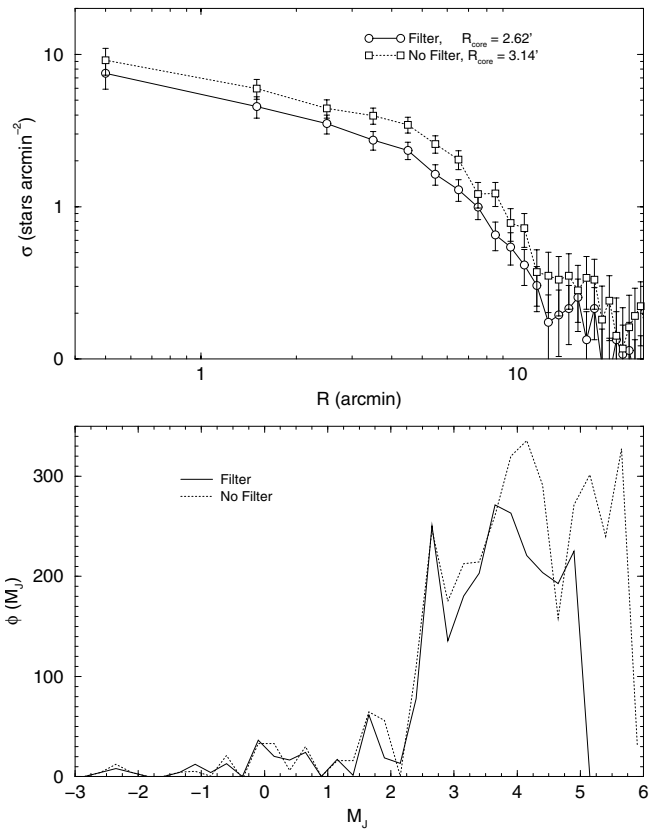

Fig. A.2. *Top panel*: background-subtracted radial distribution of stars. *Bottom panel*: overall LFs.

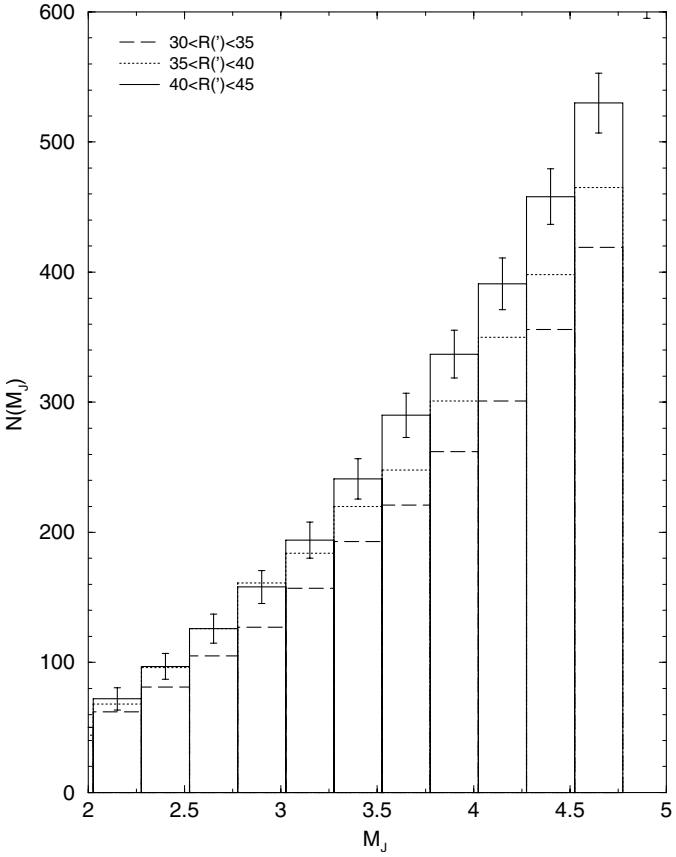

Fig. A.3. Cumulative distribution of stars in external regions of NGC 188. Dashed line: 30′−35′; Dotted line: 35′−40′; Solid line: 40′−45′. Poisson error bars for the outermost distribution are shown.

We conclude that the use of a colour filter on a CMD does not introduce significant bias or artifacts either in the radial distribution of stars or in the LF of a star cluster, at least for those clusters resembling NGC 188. Besides, the changes introduced by filters are expected to occur in the right direction, since they account for the background contamination.

Background selection and subtraction is another critical step in the analysis of star clusters. Ideally, the offset field should represent the background stellar contribution to the cluster field, both in number and spectral type distribution. This is crucial in particular for highly dynamically evolved clusters in which a significant fraction of the low-mass stars are dispersed in the external regions. For these clusters the offset field selection should be guided by a compromise between distance from the cluster border and representativeness of the background stars.

The uniform sky coverage of 2MASS provides a means to suitably account for the stellar background. We illustrate this process in Fig. A.3, in which we show the cumulative distribution of stars for three circular, external regions of NGC 188, 30′−35′, 35′−40′, 40′−45′. The first two distributions have been scaled to match the area of the outermost distribution.

Within the number fluctuation represented by the Poisson error bars, the three distributions are similar, which reflects the near uniformity of the stellar content around NGC 188. However, more internal distributions present a slight excess of low-mass stars with respect to the outermost distribution, which may be accounted for by the long-term effects of mass segregation near the tidal radius. For this reason we selected the region 40′−45′ to represent the stellar background for NGC 188.

References

Adams, F. C. 2000, ApJ, 542, 964
Allen, C., & Martos, M. A. 1988, Rev. Mex. Astron. Astrofis., 16, 25
Anthony-Twarog, B. J., Twarog, B. A., Heim, E. A., & Caldwell, N. 1991, AJ, 102, 1056
van den Bergh, S., & Sher, D. 1960, PDDO, 2, 203
Bergond, G., Leon, S., & Guibert, J. 2001, A&A, 377, 462
Bica, E., Bonatto, C. J., & Dutra, C. M. 2003, A&A, 405, 901
Bica, E., Bonatto, C. J., & Dutra, C. M. 2004, A&A, 422, 555
Binney, J., & Tremaine, S. 1987, in Galactic Dynamics (Princeton, NJ: Princeton University Press)
Binney, J., & Merrifield, M. 1998, in Galactic Astronomy (Princeton, NJ: Princeton University Press), Princeton series in astrophysics, QB857.B522
Bonatto, C., & Bica, E. 2003, A&A, 405, 525
Bonatto, C., Bica, E., & Girardi, L. 2004a, A&A, 415, 571
Bonatto, C., Bica, E., & Pavani, D. 2004b, A&A, 427, 485
Caputo, F., Chieffi, A., Castellani, V., et al. 1990, AJ, 99, 261
Carraro, G. 2002, A&A, 385, 471
Carraro, G., & Chiosi, C. 1994, A&A, 288, 751
Carraro, G., Chiosi, C., Bressan, A., & Bertelli, G. 1994, A&AS, 103, 375
Dinescu, D. I., Girard, T. M., van Altena, W. F., Yang, T.-G., & Lee, Y.-W. 1996, AJ, 111, 1205
Dutra, C. M., Santiago, B. X., & Bica, E. 2002, A&A, 381, 219
Friel, E. D. 1995, ARA&A, 33, 381
de la Fuente Marcos, R. 1998, A&A, 333, L27
de la Fuente Marcos, R., & de la Fuente Marcos, C. 2002, Ap&SS, 280, 381
Girardi, L., Bertelli, G., Bressan, A., et al. 2002, A&A, 391, 195
Harris, W. E. 1996, AJ, 112, 1487
Hernandez, X., Valls-Gabaud, D., & Gilmore, G. 1999, MNRAS, 304, 705
von Hippel, T., & Sarajedini, A. 1998, AJ, 116, 1789
Hobbs, L. M., Thorburn, J. A., & Rodriguez-Bell, T. 1990, AJ, 100, 710
Hurley, J., & Tout, A. A. 1998, MNRAS, 300, 977
Keenan, D. W., Innanen, K. A., & House, F. C. 1973, AJ, 78, 173
Kerber, L. O., Santiago, B. X., Castro, R., & Valls-Gabaud, D. 2002, A&A, 390, 121
King, I. 1962, AJ, 67, 471
King, I. 1966a, AJ, 71, 64
King, I. 1966b, AJ, 71, 276
Kroupa, P. 2002, Science, 295, 82
Kroupa, P. 2001, MNRAS, 322, 231
Kroupa, P., Tout, C. A., & Gilmore, G. 1991, MNRAS, 251, 293
Kuiper, G. P. 1935, PASP, 47, 15
Leonard, P. J. T., & Linnell, A. P. 1992, AJ, 103, 1928

Mazeh, T., Simon, M., Prato, L., Markus, B., & Zucker, S. 2003, ApJ, 599, 1344
Mermilliod, J. C. 1996, in The origins, evolution, and destinies of binary stars in clusters, ASP Conf. Ser., 90, 475
Montgomery, K. A., Marschall, L. A., & Janes, K. A. 1993, AJ, 106, 181
Nissen, P. E. 1988, A&A, 199, 146
Norris, J., & Smith, G. H. 1985, AJ, 90, 2526
Oh, K. S., & Lin, D. N. 1992, ApJ, 386, 519
Pavani, D. B., Bica, E., Dutra, C. M., et al. 2002, A&A, 374, 554
Pavani, D. B., Bica, E., Ahumada, A. V., & Clariá, J. J. 2003, A&A, 399, 113
Sandage, A. R. 1961, AJ, 66, 53
Sandage, A. R. 1962, ApJ, 135, 349
Sarajedini, A., von Hippel, T., Kozhurina-Platais, V., & Demarque, P. 1999, AJ, 118, 2894
Skrutskie, M., Schneider, S. E., Stiening, R., et al. 1997, in The Impact of Large Scale Near-IR Sky Surveys, ed. Garzon et al. (Netherlands: Kluwer), 210, 187
Soares, J. B., & Bica, E. 2002, A&A, 388, 172
Takahasi, K., & Portegies Zwart, S. F. 2000, ApJ, 535, 759
Trager, S. C., King, I. R., & Djorgovsky, S. 1995, AJ, 109, 218
Twarog, B. A. 1978, ApJ, 220, 890
Twarog, B. A., Ashman, K. M., & Anthony-Twarog, B. J. 1997, AJ, 114, 2556
Wielen, R. 1991, in The Formation and Evolution of Star Clusters, ed. K. Janes, ASP Conf. Ser., 13, 343